DETECTING UNMARKED MOOSE WITH INFRARED SENSORS VIA AN UNOCCUPIED AERIAL SYSTEM AND CORRECTING FOR SIGHTABILITY

Lily M. Hall[1*], Franklin B. Sullivan[2], Sophia A. Burke[2], Michael W. Palace[2,3], Henry Jones[4], and Remington J. Moll[1]

[1]Department of Natural Resources and the Environment, University of New Hampshire, 56 College Road, Durham, NH 03824, USA; [2]Earth System Research Center, University of New Hampshire, 8 College Rd, Durham NH 03824, USA; [3]Department of Earth Science, University of New Hampshire, 56 College Road, Durham, NH 03824, USA; [4]New Hampshire Fish & Game Department, 629B Main Street, Lancaster, NH 03584, USA

*Corresponding author: Lily M. Hall, lilymhall32@gmail.com

ABSTRACT: Accurate and precise estimates of moose (*Alces alces*) density are pivotal for understanding population dynamics and informing management decisions. One promising tool for obtaining this information is unoccupied aerial systems (UASs). However, this technology still requires critical evaluation, especially regarding properly accounting for imperfect detection, i.e., the probability that moose are available but not detected and therefore uncounted. A recent review found that less than half of studies estimating moose density adequately accounted for imperfect detection, suggesting that many moose populations might be underestimated. Our objective was to create a sightability model for unmarked moose detected from a UAS equipped with a long-wave infrared sensor that included covariates expected to affect large-scale UAS moose surveys. We conducted 35 UAS flights in northern New Hampshire, USA, during January and February 2023 and completed sightability maneuvers over 59 moose detections to collect images at various relative observation angles. From a Bayesian logistic regression based on a naïve observer analysis, we found that greater conifer cover and sunnier conditions strongly reduced sightability of moose whereas ambient temperature had a weaker but also negative effect. Sightability was near 100% below a threshold of approximately 50% conifer cover, above which sightability declined rapidly which is similar to findings from previous work. This study provides the first successful quantification of sightability for a non-collared moose population, demonstrating a cost-effective approach for calibrating UAS sampling for additional locations and species while paving the way for future applications of this model to correct moose population sampling.

ALCES VOL. 60: 147 – 165 (2024)

Key Words: *Alces alces*, drone, imperfect detection, moose, sightability, thermal, ungulate, unoccupied aerial system (UAS)

Estimating animal density and monitoring densities over time are pivotal for understanding population dynamics and for making informed management decisions, especially for charismatic and harvested species impacted by emerging threats like climate change (Dice 1938, Sala et al. 2000, Fryxell et al. 2014). Moose (*Alces alces*) are one such species given their intensive management as a game animal, their susceptibility to expected climate change effects, and their overall public interest (Boutin 1992, Rempel et al. 1997, Musante et al. 2010, Jones et al. 2019, Ruprecht et al. 2020, Moll et al. 2022). Beyond general ongoing work to monitor moose as a game species, recent

research effort has also focused on predicting potential range shifts of moose in response to climate change (Tape et al. 2016, Teitelbaum et al. 2021) and understanding moose population responses to parasitism by winter ticks (*Dermacentor albipictus*) (Jones et al. 2019, Ellingwood et al. 2020, DeBow et al. 2022). Topics like these would be further illuminated by obtaining improved spatially explicit density estimates for moose populations throughout their range (Michaud et al. 2014, Hinton et al. 2022). Such estimates have traditionally come through ground surveys of tracks or pellets or from aerial surveys using helicopters or fixed-winged aircrafts (e.g., Gasaway et al. 1986, Kretser et al. 2016). However, these methods can be prohibitively time- and cost-intensive, and the predominant method – aerial surveys – is limited to optimal winter weather conditions that are diminishing due to climate warming (Brinkman et al. 2024). Considering logistical demands, these methods can limit the spatial scale and temporal resolution of data that researchers and managers use to monitor moose (Rahman and Rahman 2021, Moll et al. 2022). Other more cost-effective monitoring techniques exist, including the use of public reports and harvest data analyses. However, these approaches require careful and periodic calibration using independent datasets (Bontaites et al. 2000) and can be limited to areas with sufficient harvest (Solberg et al. 1999) or hunter observers (Boyce and Corrigan 2017) and thus often warrant supplementation through other monitoring methods.

Recent technological developments in unoccupied aerial systems (UASs) hold promise for efficiently obtaining spatially explicit moose density estimates as well as increasing the temporal resolution of data while remaining at an accessible cost for many research entities (Anderson and Gaston 2013, Linchant et al. 2015, Rahman and Rahman 2021, Moll et al. 2022, Elmore et al. 2023). Given that UASs can fly at lower altitudes and slower speeds than piloted aircrafts, they can provide finer resolution data (Anderson and Gaston 2013) and can be safer and more adaptable in adverse weather conditions (Zmarz et al. 2018). In addition, UASs can be readily equipped with various sensors suited to detect wildlife (Iglay et al. 2024), including long-wave infrared sensors that enable detection of individual endotherms such as moose. Although UAS studies have examined free-ranging (McMahon et al. 2021*b*, Mayer et al. 2024) and captive ungulate populations at localized spatial scales (e.g., 0.13 km^2, Zabel et al. 2023; 1.74 km^2, Beaver et al. 2020), UAS surveys have generally not been conducted at larger spatial scales (Wang et al. 2019). An exception was a large-scale evaluation of kangaroo monitoring that concluded UAS surveys were an unsuitable replacement for their helicopter surveys, partially due to insufficient resolution of infrared imagery for species identification (Gentle et al. 2018). However, improvements in UAS, battery, and infrared sensor technologies have extended flight times and increased image resolution, making UASs a promising solution for monitoring species on broader spatial scales (Linchant et al. 2015, Cleguer et al. 2021), particularly for moose monitoring where species differentiation is more distinct. Nevertheless, difficulties related to environmental conditions such as snow presence, thermal contrast, and vegetation obstruction must be navigated (Havens and Sharp 2015, Burke et al. 2019). A limitation of UAS sampling in the USA is the availability of launch locations with sufficient visibility to comply with the Federal Aviation Administration requirement to maintain visual line-of-sight (VLOS) with the system during flight (FAA 2024). The availability of such launch locations will

vary by land cover and is expected to be rarest in tall, dense conifer-dominated forests. Therefore, although UASs are a promising new technology for monitoring moose and other wildlife species, their use requires further field validation.

As for any wildlife survey attempting accuracy, a critical component of moose surveys is accounting for imperfect detection by estimating the probability of detecting a study animal that is present on a transect or sample plot (Caughley 1974, MacKenzie et al. 2002, Tyre et al. 2003, Cleguer et al. 2021). After biologists quantify this probability, they can apply a sightability correction factory (SCF; (Gasaway et al. 1986, Steinhorst and Samuel 1989) to their population estimate which is crucial for obtaining accurate abundance data (Guillera-Arroita et al. 2014) and obtaining reliable inference about species occurrence and wildlife-habitat relationships (Kéry et al. 2010). Although sightability corrections are particularly relevant to reducing bias due to undercounting, it is critical to also understand the potential of overcounting based on sampling design and animal movement (Schultz et al. 2024). Imperfect detection of moose has previously been addressed using double observers (Cumberland 2012, Kantar and Cumberland 2013, Oyster et al. 2018), calibrations with infrared technology (Bontaites et al. 2000), and quantifying detection probability via radio- or GPS-collared individual moose (Peters et al. 2014, Oyster et al. 2018, McMahon et al. 2021*b*). Steinhorst and Samuel (1989) pioneered an approach to correcting for imperfect detection by modeling factors affecting detection using logistic regression that has come to be known as sightability modeling. However, many studies estimating moose populations (including aerial, ground, and public surveys) have not accounted for imperfect detection. For example, a recent review of 89 moose monitoring studies found that only 36% explicitly accounted for imperfect detection and that accounting for detection bias had not improved over time (Moll et al. 2022). This lack of explicitly accounting for imperfect detection is particularly concerning as even moose sightability models with similar covariates have been shown to produce very different corrected population estimates (e.g., 5.6x different, Harris et al. 2015). Furthermore, evaluations of emerging infrared detection technology as an aerial surveying method (e.g., infrared detectors on UASs) have only recently been conducted (McMahon et al. 2021*a*, *b*; Delisle et al. 2023; Zabel et al. 2023) and are rare for moose (Elmore et al. 2023). Despite this, UASs equipped with infrared sensors can detect moose accurately in some conditions, with up to an 85% detection rate when flying in conditions that maximize thermal contrast such as cooler parts of the day and overcast skies (McMahon et al. 2021*b*). However, detection probability declines sharply with canopy closure which in the winter is often due to the presence of conifer trees (Peters et al. 2014, Oyster et al. 2018, McMahon et al. 2021*b*).

Two studies have examined moose detection probability using infrared imagery with UASs (McMahon et al. 2021*b*, Mayer et al. 2024). Here, we build upon these initial assessments to create a sightability model of unmarked moose detected from a UAS equipped with an infrared sensor. We used naïve observer detections of known moose to examine a Bayesian logistic regression model that incorporated biotic and abiotic covariates that we hypothesized to influence moose sightability (Table 1). These covariates, including temperature, cloud cover, and conifer cover, would be expected to affect any large-scale UAS moose survey. Our results provide a model for use in future sampling surveys to estimate spatially

Table 1. Covariate hypothesis, name of covariate, description of data used in modeling to operationalize the covariate hypothesis, the predicted positive (+) or negative (-) effect of the covariate on moose sightability, and relevant references for hypotheses evaluated for predicting moose sightability from infrared images collected via an unoccupied aerial system for moose in New Hampshire, USA, winter 2023. A summary of the data is included in the covariate column.

Covariate hypothesis	Covariate	Data description	Predicted effect	References
The thick canopy of conifer trees obscure infrared sensing of objects below	Percentage of conifer cover (min = 24, max = 85, mean = 61, SD = 18)	The percentage of the RGB image pixels identified as conifer via GLI	-	Kissell and Nimmo 2011, Peters et al. 2014, Oyster et al. 2018, McMahon et al. 2021b, Hinton et al. 2022
Thermal contrast between moose and the environment decreases as temperature increases reducing visibility	Ambient temperature (min = -8.9, max = 2.2, mean = -1.7, SD = 3.1)	The ambient temperature in °C during image collection	-	Street et al. 2015, Hinton et al. 2022, Zabel et al. 2023
Ambient temperature and temperature of objects in the environment increase with time since sunrise, decreasing thermal contrast	Time of day (min = 6.0, max = 16.0, mean = 11.0, SD = 2.6)	The hour of the day rounded down to the whole hour	-	Zabel et al. 2023
Cloud cover blocks solar radiation, increasing thermal contrast	Cloud cover (n = 707 overcast; n = 158 partly sunny)	Categorical degree of cloud cover at the start of image collection	+	Millette et al. 2011, McMahon et al. 2021b, Mayer et al. 2024
Temperatures decrease into February and increase thermal contrast	Day of year (min = 16, max = 46, mean = 27, SD = 6.3)	Julian day of image collection	+	Quayle et al. 2001, Zabel et al. 2023
Fewer observation angles reduce the chance of the moose being detected due to environmental obstruction	Unequal (n = 420 unequal; n = 445 equal)	Whether or not the sequence had moose not in the viewshed for all 3 images	-	Coates et al. 2019

explicit moose densities that will be useful for informing moose management and guiding the application of UAS infrared technologies to other systems.

STUDY AREA

We conducted UAS flights from 5 launch sites in northern New Hampshire, USA, in New Hampshire Fish and Game Wildlife Management Units A1, C1, and C2 (NHFG 2023). The study area was mostly forested with low levels of anthropogenic development; land cover consisted of approximately 91% forest (16% conifer, 34% deciduous, and 41% mixed), 3% developed, 3% shrub/scrub land, and 2% water (Dewitz 2020). The predominant forest type was northern hardwood-conifer forest consisting mainly of maple (*Acer* spp.), birch (*Betula* spp.), and American beech (*Fagus grandiflora*) with lowland and high elevation spruce-fir forests of primarily red spruce (*Picea rubens*) with intermixed balsam fir (*Abies balsamea*; DeGraaf and Yamasaki 2001, NHFG 2015, Jones et al. 2019). Launch location elevations ranged from 400 to 700 m. Snowfall during the study period was 95 cm with a mean temperature of -5°C while

the 1991 - 2020 average annual temperature was 6°C (NOAA 2024). The area was considered high quality moose habitat with the 2022 estimated moose densities ranging from 0.6 - 3.5 moose/km^2 across the region (NHFG 2023).

Landownership included state owned parks, privately owned land, and commercially logged forests. We secured written permission from all landowners to collect data from a UAS prior to flying. To maximize the area covered per flight, we focused sampling in Jericho Mountain State Park (latitude: 44.47, longitude: -71.26) which provided optimal launch locations due to a clear view over the canopy from across a large lake (Jericho Lake) and also enabled us to adhere to the Federal Aviation Administration regulation of maintaining a visual line-of-sight of the UAS during flights.

METHODS

UAS Data Collection

During January and February 2023, we conducted 35 UAS flights using a DJI Matrice 300 RTK quadcopter (Shenzhen DJI Sciences and Technologies Ltd., Nanshan District, Shenzhen, China) equipped with a DJI Zenmuse H20T sensor perpendicular to the ground recording color (RGB; 4056 x 3040 pixels, 82.9° DFOV) and long-wave infrared thermal images (640 x 512 pixels, 40.6° DFOV). For each flight, we confirmed consistent snow cover but did not have a required minimum depth and recorded ambient temperature (°C), relative humidity, and windspeed (mph) at the beginning of the sightability maneuver with a handheld Kestrel 5500 weather station (Kestrel Instruments, Boothwyn, Pennsylvania, USA) and noted time of day and sky condition as potential categories of overcast, partly sunny, sunny, or dark.

We started flights by following pre-programmed, terrain-following lawnmower pattern flight paths created in UgCS (v. 4.8.728, Smart Projects Holding, Ltd., Valletta, Malta) and imported to DJI Pilot 2 (Shenzhen DJI Sciences and Technologies Ltd., Nanshan District, Shenzhen, China) as KML files with the objective of detecting moose for further data collection as opposed to abundance sampling. We set photogrammetry mission parameters targeting 10 cm resolution for thermal images, 20% side overlap, and 33% forward overlap to balance the goals of searching as much area as possible while having sufficient detectability for moose. This resulted in flying at ~ 100 m altitude at 8 m/s while recording images every 2 seconds. After we detected a moose, we manually flew a set pattern known as a sightability maneuver to mimic intensive flights in previous studies (Gasaway et al. 1986, Poole et al. 1999, Bontaites et al. 2000). These flights assumed a 100% detection rate by increasing sampling effort (e.g., flying lower or slower) to generate an abundance estimate to which the corresponding sampling flight (e.g., flying faster or at higher altitudes) would be compared. Our sightability maneuvers made repeated flights at ~ 100 m altitude over confirmed moose detections (i.e., true positives; n = 59) that would later be used to estimate moose sightability in a naïve observer analysis. During the sightability maneuvers, we captured simultaneous infrared and RGB images with the sensor downward-facing (i.e., nadir) and manipulated the flight patterns to position moose detections across all areas of the sensor viewsheds (i.e., in the left, right, top, bottom, center, and all corners of a square viewshed). We also flew true negative sightability maneuvers over the locations where true positive sightability maneuvers were conducted at least 6 days after the moose left. These true negative maneuvers

enabled us to assess detection rates across identical vegetation conditions, thereby controlling for unmeasured factors related to landscape features.

Finally, we estimated the percentage of conifer cover for all images captured during flights by: (1) retrieving and clipping a corresponding wide view RGB image to the footprint of the thermal image; (2) calculating the median Green Leaf Index (GLI, Eq. 1, e.g. Louhaichi et al. 2001) of a 25-pixel window around each pixel; and (3) calculating the proportion of all pixels in the image with a GLI ≤ 0.75.

$$GLI = ((GDN - RDN) + (GDN - BDN)) / ((2*GDN) + RDN + BDN) \quad \text{(Eq. 1)}$$

where DN is the digital number of each band (i.e., Blue, Green, and Red) preceded by an identifier of the band (B, G, and R respectively). GLI is a useful index for detecting chlorophyll content of leaves and vegetation because chlorophyll absorbs blue and red wavelengths and reflects green wavelengths (Louhaichi et al. 2001, Macfarlane and Ogden 2012, Bush et al. 2020). This GLI threshold approach has been previously applied to winter optical imagery as a simple method to differentiate conifer and deciduous canopy vegetation (Sullivan et al. 2023).

Naïve Observer Analysis

We randomly selected 300 infrared images with moose as true positives and 300 without moose as true negatives (i.e., controls that lacked moose) for the naïve observer analysis. The true positive images were in three-image sequences to create 100 sequences, with each sequence displaying 1 focal moose being moved down each third of the image viewshed to replicate the changes in perspectives that occur for an observer during forward flight. Similarly, we prepared 100 true negative image sequences by choosing a focal ground location instead of a focal moose to display. The sequences were distributed so each vertical third of the viewshed was represented evenly. Percentage of conifer cover was also distributed evenly across the possible 0 – 100% range by leveraging multiple sequences from some trials, although values in the extreme regions of the percentage of conifer cover (below 23% and above 85% conifer cover) were not surveyed in the field and thus not available. We anonymized and randomized the thermal and RGB images from true positive and true negative sightability maneuvers using package magick (Ooms 2024) in R (version 4.2.1; R Core Team 2024). We then provided the infrared images to naïve observers using the program timelapse (https://timelapse.ucalgary.ca, version 2.3.0.6; Greenberg et al. 2019).

We trained naïve observers (n = 11) to identify moose in infrared image sets via a 45-minute video (see Supplemental Material) containing explanations on image features useful for identifying moose (i.e., shape, size, contrast from background, tracks). We overlaid a light gray 3 x 3 rectangle grid over the infrared images and compared the true moose presence to the naïve observer recorded moose presence in each of the 9 cells. This defined a smaller area to help determine if a naïve observer identified a moose in the image as opposed to a non-moose feature. These observers had no prior knowledge of image locations or whether an image contained a moose (McMahon et al. 2014). Naïve observers had the option to examine both the infrared images and the corresponding RGB images during training and analysis (Fig. 1). We permitted naïve observers to examine RGB images at their discretion because we determined it helpful

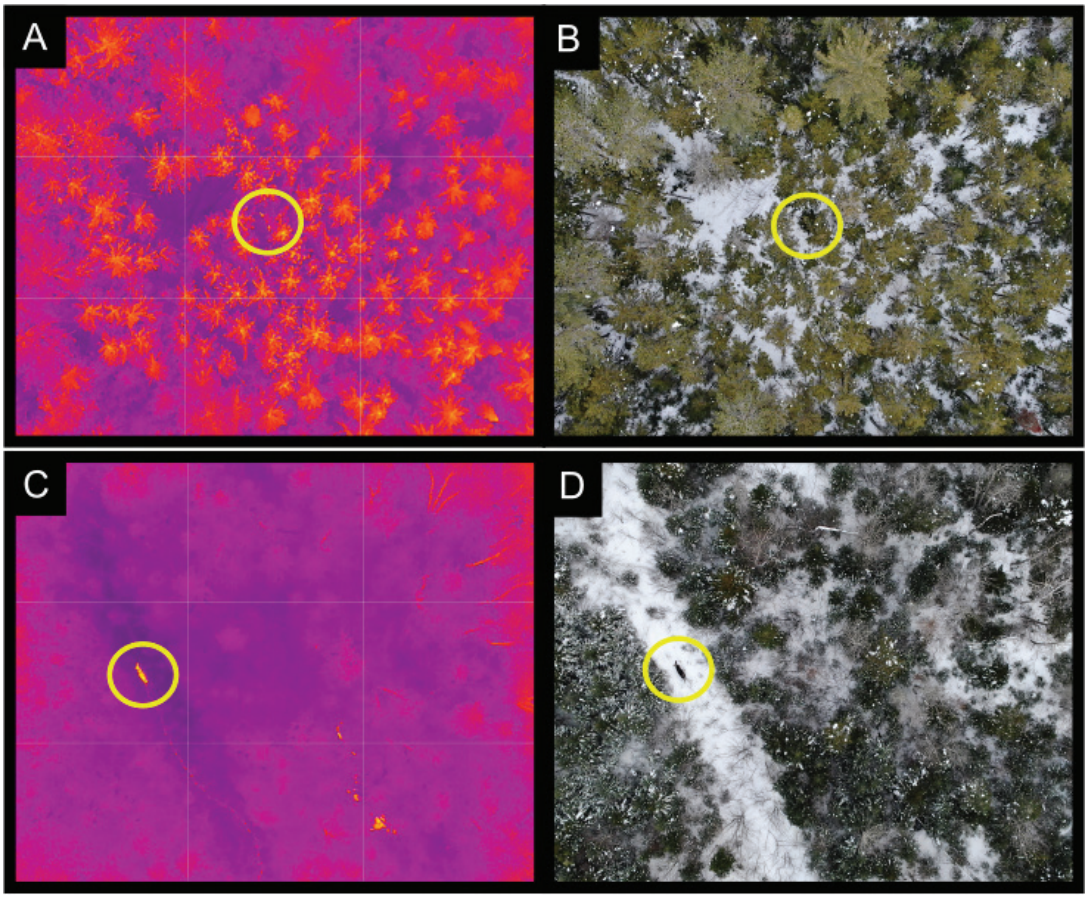

Fig. 1. Corresponding long-wave infrared (A & C) and RGB (B & D) images captured while conducting UAS sightability maneuvers over moose (located within the yellow circles) in northern New Hampshire, USA, winter 2023. Each pair of images was captured simultaneously at the same location over either a high (A & B) or low conifer area (C & D), illustrating variation in moose sightability. The infrared images include a light gray 3 x 3 rectangle grid used in the naïve observer analysis to aid in image tracking. Image C also shows moose tracks in snow which was one sign naïve observers were trained to use as an aid in moose detection.

in improving the accuracy of moose identification, particularly when a moose bed was present that often showed a similar signature in the infrared image to a moose. We included multiple naïve observers so that we could account for observer-level differences in detection rates (Attard et al. 2024).

Prior to analyzing the naïve observer data to estimate moose sightability by correcting for false negatives, we first determined if naïve observers recorded any false positives (i.e., identified moose that were not present) to confirm that such detections did not occur at a rate warranting inclusion in the model. False positives occurred < 1% of the time and this rate was too low to formally include in the sightability model. Additionally, in 10 out of the 875 sequences (1%), naïve observers recorded more moose than were present (e.g., a naïve observer recorded 3 moose when only 2 were present). We excluded these false positives in the sightability model as well, but we discuss these false positive rates when

providing recommendations for future UAS work. After each naïve observer processed the 600 moose images (200 sequences of 3 images), we realized that during our sightability maneuvers (which we conducted following a zig-zag pattern from top-to-bottom, left-to-right), moose had more time to move between vertically sequential images than there would be in a traditional transect sampling approach. To maximize the applicability of our sightability model, we removed sequences in which moose moved more than 30% of the image length throughout the sequence (n = 5). We also removed images collected in the dark (n = 8) because flights pre- and post-sunrise were logistically difficult but did not seem to increase the thermal signature of moose. We therefore conducted the final sightability analysis on 261 unique true positive images (87 unique sequences).

Sightability Model Description

We analyzed the proportion of moose that naïve observers correctly identified (i.e., sightability) in true positive sequences using a binomial logistic regression model. We included covariates that we hypothesized would affect sightability in the linear predictor of the model (Table 1), as follows:

$$\text{mooseDet}_i \sim \text{Binomial}(p_i, N_i)\ \text{logit}(p_i) = \beta_{NO[i]} + \beta.Con_{NO[i]} * \text{Con}_i + \beta.Time_{NO[i]} * \text{Time}_i + \beta.Day_{NO[i]} * \text{Day}_i + \beta.Temp_{NO[i]} * \text{Temp}_i + \beta.Unequal_{NO[i]} * \text{Unequal}_i + \beta.Cloud_{NO[i]} * \text{Cloud}_i \quad \text{(Eq. 2)}$$

where mooseDet_i was the number of total moose that the naïve observer successfully detected in the i^{th} image sequence given p_i as the probability of success (i.e., correctly identifying a moose that was truly present, also referred to as sightability) and a true number of moose, N_i. In this model formulation, each true positive sequence (n = 87 per naïve observer) served as a data point composed of N_i independent trials of moose detection, each with binary responses (detected or not). The intercept and each covariate effect (i.e., the βs) were all indexed by naïve observer (NO[i]) because we modeled these parameters as random effects to account for potential pseudo-replication due to different naïve observers processing the same image sequences. Accordingly, we made inference on parameters averaged across all naïve observers (i.e., the posterior of the random effect; see below). Con_i, Time_i, Day_i, Temp_i, Unequal_i, and Cloud_i were covariate values for the i^{th} image sequence for percentage of conifer cover, hour of the day, day of the year, ambient temperature (°C), categorical classification of whether the number of moose were equal across all 3 images, and cloud cover (overcast or partly sunny, as dark images were removed and no moose were encountered in sunny conditions), respectively. We included the unequal covariate to account for sequences with an unequal number of moose per image (i.e., 1 moose might have only been present in 1 or 2 images in the sequence of 3 because a second moose was the one we targeted to be in each third of the viewshed). This situation would not arise with typical field data where the sampling transect would continue, so this covariate controlled for the nuisance effect of reduced number of observation angles for some moose to avoid bias in the sightability model.

We used the package car (Fox et al. 2024) to check for collinearity between covariates by first identifying covariates with an adjusted generalized standard error inflation factor (aGSIF) > 1.7, which is comparable to a variable inflation factor (VIF) >3 (Fox and Monette 1992, Zuur et al. 2010). We also initially considered a nonlinear effect (Heit et al. 2024) of time of day by including a Time^2 covariate to test the

Table 2. Estimates of the effects of scaled covariates on moose sightability from a binomial logistic regression fit to unoccupied aerial system data, winter 2023, New Hampshire, USA. Intercepts represent the sightability of moose on the logit scale with overcast skies and an equal number of moose in all image sequences. An asterisk (*) indicates significant terms (95% credible interval (CI) does not include zero).

	Posterior Mean	Lower 95% CI	Upper 95% CI
Intercept	1.43*	0.71	2.15
Percentage of conifer cover	-1.51*	-1.96	-1.15
Time of day	0.16	-0.08	0.42
Day of year	-0.27*	-0.56	-0.01
Ambient temperature	-0.24*	-0.41	-0.07
Unequal presence of moose within the image sequence	-0.36	-0.81	0.04
Cloud cover	-1.81*	-2.28	-1.37

hypothesis that time had a quadratic relationship with moose sightability due to changing sunlight and temperatures throughout the day. However, Time and Time^2 had a GSIF > 1.7, thereby introducing collinearity, and models including both terms did not converge in the Bayesian analysis described below. Prior to omitting Time^2 from further consideration, we examined a frequentist version of the global model with and without the term and found no support for retaining Time^2 based upon AIC (ΔAIC < 2; Arnold 2010). We therefore removed Time^2 from further analysis, which resulted in all remaining covariate aGSIFs < 1.7.

We analyzed the model using Markov Chain Monte Carlo (MCMC) simulations in a Bayesian framework. We used R to run the model in JAGS language with R2jags (Su and Yajima 2024). For the final model evaluation, we used 3 MCMC chains of 10,000 iterations each with a burn-in of 1,000 and a thinning rate of 1 (Link and Eaton 2012). We used diffuse logistic distribution priors for all covariate parameters and scaled the covariates to facilitate comparison of effect sizes across covariates (Northrup and Gerber 2018). We confirmed model convergence by visually inspecting traceplots and ensuring that *R*-hat statistics were < 1.1 (Gelman and Hill 2007). We assessed model fit using Bayesian p-values using standard techniques (Kéry and Royle 2015). To do so, we compared the Pearson residuals from field-collected data to those calculated from model-predicted data. We considered model fit acceptable if the Bayesian p-value was $0.05 \leq p \leq 0.95$ and excellent if the value was near 0.5, which would indicate that the model could faithfully reproduce the field data (Kéry and Royle 2015). We interpreted models by evaluating covariate effects (β values in Eq. 2) for significance, defined as whether the 95% credible interval contained zero or not (Kéry and Royle 2015).

RESULTS

Naïve observers correctly identified 1,074 of the 1,633 moose (66%) across 865 true positive sequences of long-wave infrared images. A Bayesian p-value of 0.46 indicated that the model described above provided an excellent fit to these data. We found that percentage of conifer cover had strong and significant negative effects on moose sightability (Table 2; standardized β posterior mean = -1.51). Sightability was near 100% below a threshold of approximately 50% conifer cover, above which sightability declined rapidly (Table 2; Fig. 2a). We also found that ambient temperature had a significant but relatively modest negative effect

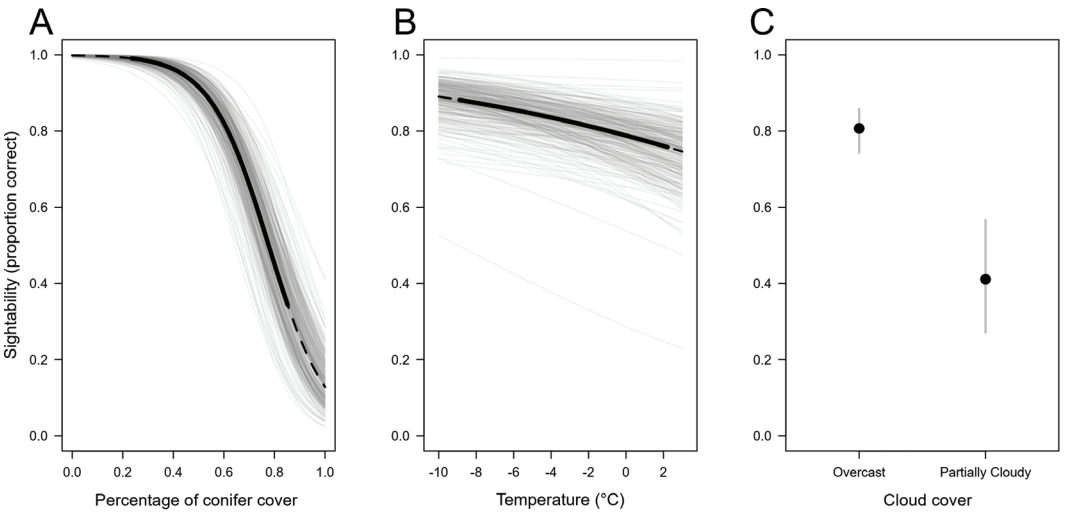

Fig. 2. Model-predicted sightability (probability of correctly detecting a moose) as a function of A) percentage of conifer cover, B) ambient temperature, and C) cloud cover based upon a binomial logistic regression model fit to data collected by an unoccupied aerial system during winter 2023, New Hampshire, USA. Solid black line represents mean predicted sightability, light grey lines depict uncertainty, and dashed lines depict extrapolated model predictions beyond the range of field data values.

(standardized β posterior mean = -0.24) on sightability, which declined approximately 10-15% as temperature increased from -10° to 4° C (Table 2; Fig. 2b). Cloud cover had a strong effect on sightability (Table 2; Fig. 2c), with mean sightability during overcast conditions (80.8%) nearly double that during partly sunny conditions (40.6%). Day-of-year had a negative effect on sightability, but the relationship was modest (standardized β posterior mean = -0.27) and the 95% credible interval very nearly overlapped zero (upper bound of -0.01). The model did not detect an effect of time-of-day or unequal presence of moose (Table 2). For the original 198 true positive and true negative sequences given to all observers, naïve observers accessed the RGB images in 11% of the sequences (232 of 2178 sequences). The observers changed their moose identification decision based on information from the RGB images in 2% of the sequences (52 of 2178 sequences).

DISCUSSION

We created a sightability model for unmarked moose from a naïve observer analysis of long-wave infrared images captured via a UAS. Because our flights were conducted during winter with snow cover and deciduous leaf-off, moose were generally easy to detect as large, warm bodied individuals in infrared imagery except when in dense conifer cover. Specifically, according to a Bayesian logistic regression, we found that a greater percentage of conifer cover and sunnier sky conditions strongly reduced sightability of moose whereas ambient temperature had a weaker negative effect. Although most of these influences were expected (e.g., negative effects of conifer cover; McMahon et al. 2021b), determining location specific sightability models is important for accuracy as even models with similar covariates can greatly affect the corrected population count based on their respective coefficients (Harris et al. 2015).

Because the successful estimation of sightability for non-collared moose populations had not been completed yet (McMahon et al. 2021*b*, Mayer et al. 2024), our results are an encouraging demonstration of a cost-effective approach for calibrating UAS sampling for additional locations and species

The percentage of conifer cover, cloud cover, and ambient temperature were significant covariates in the logistic regression model. Conifer cover was influential and negatively correlated with moose detection. This was expected due to visual obstruction (Cilulko et al. 2013, Burke et al. 2019) which has been the predominant factor influencing bias of UAS imagery of wildlife (Cleguer et al. 2021, Elmore et al. 2023) and previous findings of canopy cover effects (Chrétien et al. 2016, Doull et al. 2021, McMahon et al. 2021*b*, Mayer et al. 2024). The influence of the percentage of conifer cover quantified as a relatively small area (40 m x 60 m viewing area of each image) highlights the importance of examining fine-scale covariates when accounting for sightability of wildlife during larger scale population sampling efforts. These fine-scale effects are likely because the conifer trees immediately surrounding the moose determine whether the moose is visible or not from above. However, future studies applying a sightability model to population sampling could build on our results by examining the scale of effect (Holland et al. 2004, Levin 1992, Wiens 1989) of percentage of conifer cover especially when considering varying levels of forest patchiness. Our observation of conifer cover effects is similar to, but slightly weaker than, that reported by McMahon et al. (2021b) for UAS field trials conducted with collared moose in Minnesota, USA. Additionally, overcast days have been shown to significantly increase moose detection with infrared sensors compared to sunny days (McMahon et al. 2021*b*, Mayer et al. 2024). This effect is likely caused by cloud cover reducing thermal loading which in turn increases the thermal contrast between the moose and its environment (Garner et al. 1995, Burke et al. 2019). In line with this expectation, we found that moose sightability was significantly greater on overcast days than on partially overcast days. Although we were unable to include sunny conditions in our model due to a lack of opportunities during data collection, we would expect sightability to be lower during full sun conditions as well. Finally, the model suggested a weak negative effect of ambient temperature which we had predicted. This effect could result when warmer ambient temperatures decrease the thermal contrast between warm moose and their environment (Garner et al. 1995). Warmer temperatures also heat up other objects such as tree trunks or rocks that could provide a bright thermal signature similar to a moose in the infrared image (Garner et al. 1995, Doull et al. 2021). Interestingly, previous studies did not include ambient temperature in their best model; however, their UAS flights were conducted in generally warmer temperatures (e.g., mean [min, max]: 14 [-1, 27 °C] McMahon et al. 2021b; 14 [9, 23 °C] Mayer et al. 2024) than ours (-2 [-9, 2 °C]). This suggests that the influence of ambient temperature may plateau at higher temperatures. We observed more thermal noise, especially around the leafless deciduous canopies during our high temperature flights, which would decrease sightability of animals on the ground.

Day-of-year, time-of-day, and unequal presence of moose had marginal or insignificant effects on sightability. Day-of-year had a significant negative effect on sightability according to our model, but the effect was highly variable and uncertain (Table 2). We had predicted that day-of-year would have a

negative effect because ambient temperatures in our study area of New Hampshire typically decrease through January with a slight increase in temperatures during the first weeks of February when we were sampling (NOAA: National Oceanic and Atmospheric Administration 1991). Additionally, environmental changes correlated with date could influence animal behavior that would influence sightability (Cilulko et al. 2013). For example, moose have been shown to preferentially travel beneath conifer trees later in winter after accumulated snow in open areas impede movement (Balsom et al. 1996). We expected this behavioral change to reduce sightability by increasing the amount of time moose are blocked by conifer cover. We did not collect snow depth data, but anecdotally, moose sightings and tracks remained prevalent in open areas throughout the study period suggesting that snow depth had not reached a threshold to noticeably shift moose habitat use to more conifer areas. Similarly, our results did not support our prediction that time-of-day (on an hourly scale) would have a negative relationship with sightability due to generally increasing temperatures after sunrise which would decrease thermal contrast. We had originally hypothesized that as temperature peaked during midday, sightability would also display this trend relative to the time of day; however, we found no support for a quadratic relationship. This lack of a trend may be because our latest sample was at 16:00 and did not adequately capture the temperature decline towards the end of the day. Time-of-day might also be important in sunnier conditions because there would be greater thermal loading on vegetation, potentially decreasing thermal contrast between vegetation and moose. Our field conditions were typically cloudy or partly sunny, so we suggest researchers in sunnier conditions still consider the possibility of time-of-day effects. We conclude that ambient temperature was more influential for sightability than day-of-year or time-of-day, although future work could provide greater clarity into these variables given their potential to covary. The predominant effect of ambient temperature would be expected given that it is more directly related to thermal contrast than time-of-day or day-of-year. Indeed, these latter 2 variables are likely coarser proxies for changes in ambient temperature. We therefore suggest that including temperature in sightability models for thermal surveys is likely sufficient to account for these dynamics unless animal behavioral changes are expected to be strong across different times of day or year. Finally, our variable unequal was included in the model as a nuisance variable to account for the potential effect of having some moose visible in fewer than all of the 3-image sequences. This would not occur in typical sampling, where all image sequences would be viewed sequentially. Overall, these effects (percentage of conifer cover introducing visual obstruction and cloud cover influencing thermal contrast) corroborate those previously found in moose sightabilty models informed by UAS thermal cameras (McMahon et al. 2021*b*, Mayer et al. 2024).

With the rapid development of artificial intelligence software, processing images with computer vision algorithms could reduce the time required for manual review (LeCun et al. 2015, Longmore et al. 2017, Lamba et al. 2019). Although not as appropriate for species found in large aggregations (Attard et al. 2024), deep learning software that could classify images into presence or absence could still prove helpful for reducing processing time of images moose (which are typically solitary). Regardless, these upcoming processing approaches will need to have human observers validate their

animal classifications to determine accuracy and precision. Currently, many UAS researchers determining sightability of wildlife from infrared sensors use a naïve observers to process images prepared by a knowledgeable observer (i.e., someone who knows which files contain the target species) to quantify influential sightability factors or compare performance to traditional methods (Spaan et al. 2019, Doull et al. 2021). Most studies have found that infrared sensors or UAS surveys improve accuracy or processing time compared to traditional methods such as visual/RGB identification, ground surveys, or piloted aircraft surveys (Hodgson et al. 2016, Seymour et al. 2017, Elmore et al. 2023). To aid in the generalization of our model for potential future applications, we accounted for differences in naïve observer behaviors and abilities by averaging our 11 observers together as a random intercept. We also trained naïve observers in identifying moose in infrared images with the a single 45-minute training video. This replicable training approach may be useful in future applications.

Our approach to quantifying sightability could be applied to population assessments either by surveying a small area and extrapolating, or by surveying a larger area (Linchant et al. 2015, Spaan et al. 2019, Elmore et al. 2023). If live counts of moose (i.e., those done in real-time via video feed in the field by UAS pilots) were found to be comparable to the sightability-corrected naïve observer counts, then it would save post-processing time of future surveys. It is also possible that video data (e.g. Baldwin et al. 2023) or live counts would improve detection compared to only viewing 3 images. To make the process more comparable to visual observers from helicopters or fixed wing aircraft, it may also be worth the time and battery for UAS operators to pause for to confirm species identification. An additional consideration for improving this approach is reducing the false positive rate, even though it was very low in this study (< 1%). Previous work with identifying humans in infrared imagery found that naïve observers had a greater rate of false negatives but fewer false positives than an automated machine learning analysis (Doull et al. 2021). Here, false positives were most commonly an empty moose bed that registered an infrared signal resembling a moose. However, moose beds that would still appear white from snow were readily distinguishable from dark brown moose in the RGB image, suggesting that false positives can be minimized by confirming moose presence in the paired RGB image if collected during adequate daylight. Similarly, fusing infrared with RGB images has been shown to improve animal identification by deep learning classification networks compared to either data type alone (Krishnan et al. 2023). Both findings highlight the benefits of utilizing a dual sensor platform.

Our study builds upon the growing body of literature showing the high potential of UASs to augment animal monitoring and population ecology studies. Moose are an excellent candidate for additional UAS monitoring because of their large body size and relative consistency of detection via infrared sensors. However, care must be taken to account for conifer and cloud cover effects given their strong influence on sightability. Sightability models such as the one presented here can be readily applied to correct future sampling, which can enable UASs to more efficiently sample larger landscapes.

ACKNOWLEDGEMENTS

We thank M. Diaz, J. Merriman, J. Vincent, R. Andruk, F. Shinost, W. Chrisman, M. Poisson, A. Butler, S. Richard, C. Dawson, E. McCay, S. Young, and M. Legagneur for data analysis

support. We also thank J. DeBow for field assistance and landowners for permitting us to conduct this research and two reviewers for their feedback that helped improve this manuscript. This work was supported by the University of New Hampshire Agricultural Experiment Station under the USDA National Institute of Food and Agriculture McIntire-Stennis Project 7003422. This is Scientific Contribution number 3071.

LITERATURE CITED

Anderson, K., and K. J. Gaston. 2013. Lightweight unmanned aerial vehicles will revolutionize spatial ecology. Frontiers in Ecology and the Environment 11:138–146.

Arnold, T. W. 2010. Uninformative parameters and model selection using Akaike's information criterion. The Journal of Wildlife Management 74: 1175–1178.

Attard, M. R. G., R. A. Phillips, E. Bowler, P. J. Clarke, H. Cubaynes, D. W. Johnston, and P. T. Fretwell. 2024. Review of satellite remote sensing and unoccupied aircraft systems for counting wildlife on land. Remote Sensing 16: 627.

Baldwin, R. W., J. T. Beaver, M. Messinger, J. Muday, M. Windsor, G. D. Larsen, M. R. Silman, and T. M. Anderson. 2023. Camera trap methods and drone thermal surveillance provide reliable, comparable density estimates of large, free-ranging ungulates. Animals 13: 1884.

Balsom, S., W. B. Ballard, and H. A. Whitlaw. 1996. Mature coniferous forest as critical moose habitat. Alces 32: 131–140.

Beaver, J. T., R. W. Baldwin, M. Messinger, C. H. Newbolt, S. S. Ditchkoff, and M. R. Silman. 2020. Evaluating the use of drones equipped with thermal sensors as an effective method for estimating wildlife. Wildlife Society Bulletin 44: 434–443.

Bontaites, K. M., K. A. Gustafson, and R. Makin. 2000. A Gasaway-type moose survey in New Hampshire using infrared thermal imagery: preliminary results. Alces 36: 69–75.

Boutin, S. 1992. Predation and moose population dynamics: a critique. The Journal of Wildlife Management 56: 116–127.

Boyce, M. S., and R. Corrigan. 2017. Moose survey app for population monitoring. Wildlife Society Bulletin 41: 125–128.

Brinkman, T. J., K. A. Kellie, A. K. Reinking, G. E. Liston, and N. T. Boelman. 2024. Changing snow conditions are challenging moose (*Alces alces*) surveys in Alaska. Wildlife Society Bulletin 48: e1555.

Burke, C., M. Rashman, S. Wich, A. Symons, C. Theron, and S. Longmore. 2019. Optimizing observing strategies for monitoring animals using drone-mounted thermal infrared cameras. International Journal of Remote Sensing 40: 439–467.

Bush, E. R., E. T. A. Mitchard, T. S. F. Silva, E. Dimoto, P. Dimbonda, L. Makaga, and K. Abernethy. 2020. Monitoring mega-crown leaf turnover from space. Remote Sensing 12: 429.

Caughley, G. 1974. Bias in aerial survey. The Journal of Wildlife Management 38: 921–933.

Chrétien, L.-P., J. Théau, and P. Ménard. 2016. Visible and thermal infrared remote sensing for the detection of white-tailed deer using an unmanned aerial system. Wildlife Society Bulletin 40: 181–191.

Cilulko, J., P. Janiszewski, M. Bogdaszewski, and E. Szczygielska. 2013. Infrared thermal imaging in studies of wild animals. European Journal of Wildlife Research 59: 17–23.

Cleguer, C., N. Kelly, J. Tyne, M. Wieser, D. Peel, and A. Hodgson. 2021. A novel method for using small unoccupied aerial vehicles to survey wildlife species and model their density distribution. Frontiers in Marine Science 8: 640338.

Coates, P. S., G. T. Wann, G. L. Gillette, M. A. Ricca, B. G. Prochazka, J. P. Severson, K. M. Andrle, S. P. Espinosa, M. L. Casazza, and D. J. Delehanty. 2019. Estimating sightability of greater sage-grouse at leks using an aerial infrared system and N-mixture models. Wildlife Biology 2019: wlb.00552.

Cumberland, R. E. 2012. Potvin double-count aerial surveys in New Brunswick: Are results reliable for moose? Alces 48: 67–77.

DeBow, J., J. Blouin, E. Rosenblatt, C. Alexander, N. Fortin, K. Gieder, J. Murdoch, and T. Donovan. 2022. Birth rates and neonate survival in a parasite rich moose population in Vermont, USA. Alces 58: 51–73.

DeGraaf, R. M., and M. Yamasaki. 2001. New England wildlife: habitat, natural history, and distribution. University Press of New England, Hanover, NH.

Delisle, Z. J., P. G. McGovern, B. G. Dillman, and R. K. Swihart. 2023. Imperfect detection and wildlife density estimation using aerial surveys with infrared and visible sensors. Remote Sensing in Ecology and Conservation 9: 222–234.

Dewitz, J. 2020. National land cover database (NLCD) 2016 products (ver. 3.0, November 2023). U.S. Geological Survey.

Dice, L. R. 1938. Some census methods for mammals. The Journal of Wildlife Management 2: 119–130.

Doull, K. E., C. Chalmers, P. Fergus, S. Longmore, A. K. Piel, and S. A. Wich. 2021. An evaluation of the factors affecting 'poacher' detection with drones and the efficacy of machine-learning for detection. Sensors 21: 4074.

Ellingwood, D., P. Pekins, H. Jones, and A. Musante. 2020. Evaluating moose Alces alces population response to infestation level of winter ticks Dermacentor albipictus. Wildlife Biology 2020: 1–7.

Elmore, J. A., E. A. Schultz, L. R. Jones, K. O. Evans, S. Samiappan, M. B. Pfeiffer, B. F. Blackwell, and R. B. Iglay. 2023. Evidence on the efficacy of small unoccupied aircraft systems (UAS) as a survey tool for North American terrestrial, vertebrate animals: a systematic map. Environmental Evidence 12: 3.

FAA: Federal Aviation Administration. 2024. 14 CFR part 107 -- small unmanned aircraft systems. https://www.ecfr.gov/current/title-14/part-107. Accessed 15 Nov 2024.

Fox, J., and G. Monette. 1992. Generalized collinearity diagnostics. Journal of the American Statistical Association 87: 178–183.

____, J., S. Weisberg, B. Price, D. Adler, D. Bates, G. Baud-Bovy, B. Bolker, S. Ellison, D. Firth, M. Friendly, G. Gorjanc, S. Graves, R. Heiberger, P. Krivitsky, R. Laboissiere, M. Maechler, G. Monette, D. Murdoch, H. Nilsson, D. Ogle, B. Ripley, T. Short, W. Venables, S. Walker, D. Winsemius, A. Zeileis, and R-Core. 2024. car: Companion to applied regression. https://cran.r-project.org/web/packages/car/index.html. Accessed 30 Sep 2024.

Fryxell, J. M., A. R. E. Sinclair, and G. Caughley. 2014. Wildlife ecology, conservation, and management. John Wiley & Sons, Hoboken, NJ.

Garner, D. L., H. B. Underwood, and W. F. Porter. 1995. Use of modern infrared thermography for wildlife population surveys. Environmental Management 19: 233–238.

Gasaway, W. C., S. D. DuBois, D. J. Reed, and S. J. Harbo. 1986. Estimating moose population parameters from aerial surveys. Biological Papers of the University of Alaska 22: 1–99.

Gelman, A., and J. Hill. 2007. Data analysis using regression and multilevel/hierarchical models. Cambridge University Press.

Gentle, M., N. Finch, J. Speed, and A. Pople. 2018. A comparison of unmanned aerial vehicles (drones) and manned helicopters for monitoring macropod populations. Wildlife Research 45: 586–594.

Greenberg, S., T. Godin, and J. Whittington. 2019. Design patterns for wildlife-related camera trap image analysis. Ecology and Evolution 9: 13706–13730.

Guillera-Arroita, G., J. J. Lahoz-Monfort, D. I. MacKenzie, B. A. Wintle, and M. A. McCarthy. 2014. Ignoring imperfect detection in biological surveys is dangerous: a response to 'fitting and interpreting occupancy models'. PLOS One 9: e99571.

Harris, R. B., M. Atamian, H. Ferguson, and I. Keren. 2015. Estimating moose abundance and trends in northeastern Washington state: Index counts, sightabilty models, and reducing uncertainty. Alces 51: 57–69.

Havens, K. J., and E. J. Sharp. 2015. Thermal imaging techniques to survey and monitor animals in the wild: a methodology. Elsevier Science & Technology, Chantilly, USA.

Heit, D. R., W. Ortiz-Calo, M. K. P. Poisson, A. R. Butler, and R. J. Moll. 2024. Generalized nonlinearity in animal ecology: Research, review, and recommendations. Ecology and Evolution 14: e11387.

Hinton, J. W., R. E. Wheat, P. Schuette, J. E. Hurst, D. W. Kramer, J. H. Stickles, and J. L. Frair. 2022. Challenges and opportunities for estimating abundance of a low-density moose population. The Journal of Wildlife Management 86: e22213.

Hodgson, J. C., S. M. Baylis, R. Mott, A. Herrod, and R. H. Clarke. 2016. Precision wildlife monitoring using unmanned aerial vehicles. Scientific Reports 6: 22574.

Holland, J. D., D. G. Bert, and L. Fahrig. 2004. Determining the spatial scale of species' response to habitat. BioScience 54: 227–233.

Iglay, R. B., L. R. Jones, J. A. Elmore, K. O. Evans, S. Samiappan, M. B. Pfeiffer, and B. F. Blackwell. 2024. Wildlife monitoring with drones: A survey of end users. Wildlife Society Bulletin 48: e1533.

Jones, H., P. Pekins, L. Kantar, I. Sidor, D. Ellingwood, A. Lichtenwalner, and M. O'Neal. 2019. Mortality assessment of calf moose (*Alces alces*) during successive years of winter tick (*Dermacentor albipictus*) epizootics in New Hampshire and Maine. Canadian Journal of Zoology 97: 22–30.

Kantar, L. E., and R. E. Cumberland. 2013. Using a double-count aerial survey to estimate moose abundance in Maine. Alces 49: 29–37.

Kéry, M., B. Gardner, and C. Monnerat. 2010. Predicting species distributions from checklist data using site-occupancy models. Journal of Biogeography 37: 1851–1862.

Kéry, M., and J. A. Royle. 2015. Applied hierarchical modeling in ecology: Analysis of distribution, abundance and species richness in R and BUGS / Volume 1, Prelude and static models. Elsevier, San Diego, California.

Kissell, R. E., Jr., and S. K. Nimmo. 2011. A technique to estimate white-tailed deer Odocoileus virginianus density using vertical-looking infrared imagery. Wildlife Biology 17: 85–92.

Kretser, H., M. Glennon, A. Whitelaw, A. Hurt, K. Pilgrim, and M. Schwartz. 2016. Scat-detection dogs survey low density moose in New York. Alces 52: 55–66.

Krishnan, B. S., L. R. Jones, J. A. Elmore, S. Samiappan, K. O. Evans, M. B. Pfeiffer, B. F. Blackwell, and R. B. Iglay. 2023. Fusion of visible and thermal images improves automated detection and classification of animals for drone surveys. Scientific Reports 13: 10385.

Lamba, A., P. Cassey, R. R. Segaran, and L. P. Koh. 2019. Deep learning for

environmental conservation. Current Biology 29: R977–R982.

LeCun, Y., Y. Bengio, and G. Hinton. 2015. Deep learning. Nature 521: 436–444.

Levin, S. A. 1992. The problem of pattern and scale in ecology: The Robert H. MacArthur award lecture. Ecology 73: 1943–1967.

Linchant, J., J. Lisein, J. Semeki, P. Lejeune, and C. Vermeulen. 2015. Are unmanned aircraft systems (UASs) the future of wildlife monitoring? A review of accomplishments and challenges. Mammal Review 45: 239–252.

Link, W. A., and M. J. Eaton. 2012. On thinning of chains in MCMC. Methods in Ecology and Evolution 3: 112–115.

Longmore, S. N., R. P. Collins, S. Pfeifer, S. E. Fox, M. Mulero-Pázmány, F. Bezombes, A. Goodwin, M. De Juan Ovelar, J. H. Knapen, and S. A. Wich. 2017. Adapting astronomical source detection software to help detect animals in thermal images obtained by unmanned aerial systems. International Journal of Remote Sensing 38: 2623–2638.

Louhaichi, M., M. M. Borman, and D. E. Johnson. 2001. Spatially located platform and aerial photography for documentation of grazing impacts on wheat. Geocarto International 16: 65–70.

Macfarlane, C., and G. N. Ogden. 2012. Automated estimation of foliage cover in forest understorey from digital nadir images. Methods in Ecology and Evolution 3: 405–415.

MacKenzie, D. I., J. D. Nichols, G. B. Lachman, S. Droege, J. A. Royle, and C. A. Langtimm. 2002. Estimating site occupancy rates when detection probabilities are less than one. Ecology 83: 2248–2255.

Mayer, M., T. Vogler, G. Ausilio, T. Kirchner, K. M. Mathisen, A. L. Evans, A. Eriksen, M. Heurich, V. Naumov, P. Wabakken, and B. Zimmermann. 2024. Drone-borne monitoring of moose. Research Report, Høgskolen i Innlandet. https://brage.inn.no/inn-xmlui/handle/11250/3115853

McMahon, C. R., H. Howe, J. van den Hoff, R. Alderman, H. Brolsma, and M. A. Hindell. 2014. Satellites, the all-seeing eyes in the sky: counting elephant seals from space. PLOS One 9: e92613.

McMahon, M. C., M. A. Ditmer, J. D. Forester. 2021*a*. Comparing unmanned aerial systems with conventional methodology for surveying a wild white-tailed deer population. Wildlife Research 49: 54–65.

McMahon, M. C., M. A. Ditmer, E. J. Isaac, S. A. Moore, and J. D. Forester. 2021*b*. Evaluating unmanned aerial systems for the detection and monitoring of moose in northeastern Minnesota. Wildlife Society Bulletin 45: 312–324.

Michaud, J.-S., N. C. Coops, M. E. Andrew, M. A. Wulder, G. S. Brown, and G. J. M. Rickbeil. 2014. Estimating moose (*Alces alces*) occurrence and abundance from remotely derived environmental indicators. Remote Sensing of Environment 152: 190–201.

Millette, T. L., D. Slaymaker, E. Marcano, C. Alexander, and L. Richardson. 2011. AIMS-thermal - a thermal and high resolution color camera system integrated with GIS for aerial moose and deer census in northeastern Vermont. Alces 47: 27–37.

Moll, R. J., M. Poisson, D. R. Heit, H. Jones, P. J. Pekins, and L. Kantar. 2022. A review of methods to estimate and monitor moose density and abundance. Alces 58: 31–49.

Musante, A. R., P. J. Pekins, and D. L. Scarpitti. 2010. Characteristics and dynamics of a regional moose *Alces alces* population in the northeastern United States. Wildlife Biology 16: 185–204.

NHFG: New Hampshire Fish and Game Department. 2015. 2015 state wildlife action plan. Annual Report, Concord, NH.

NHFG: New Hampshire Fish and Game Department. 2023. 2022 New Hampshire wildlife harvest summary. Annual Report, Concord, NH.

NOAA: National Oceanic and Atmospheric Administration. 1991. NOWData: Gorham Airport, NH, USA. Daily Climate Normals, National Weather Service. <https://www.weather.gov/wrh/climate>. Accessed 9 Dec 2024.

Northrup, J. M., and B. D. Gerber. 2018. A comment on priors for Bayesian occupancy models. PLOS One 13: e0192819.

Ooms, J. 2024. magick: advanced graphics and image-processing in R. <https://cran.r-project.org/web/packages/magick/index.html>. Accessed 30 Sep 2024.

Oyster, J. H., I. N. Keren, S. J. K. Hansen, and R. B. Harris. 2018. Hierarchical mark-recapture distance sampling to estimate moose abundance. The Journal of Wildlife Management 82: 1668–1679.

Peters, W., M. Hebblewhite, K. G. Smith, S. M. Webb, N. Webb, M. Russell, C. Stambaugh, and R. B. Anderson. 2014. Contrasting aerial moose population estimation methods and evaluating sightability in west-central Alberta, Canada. Wildlife Society Bulletin 38: 639–649.

Poole, K. G., G. Mowat, and D. Pritchard. 1999. Using GPS and GIS for navigation and mark-recapture for sightability correction in moose inventories. Alces 35: 1–10.

Quayle, J. F., A. G. MacHutchon, and D. N. Jury. 2001. Modeling moose sightability in south-central British Columbia. Alces 37: 43–54.

R Core Team. 2024. R: A Language and Environment for Statistical Computing. R Foundation for Statistical Computing.

Rahman, D. A., and A. A. A. F. Rahman. 2021. Performance of unmanned aerial vehicle with thermal imaging, camera trap, and transect survey for monitoring of wildlife. IOP Conference Series: Earth and Environmental Science 771: 012011.

Rempel, R., P. Elkie, A. Rodgers, and M. Gluck. 1997. Timber-management and natural-disturbance effects on moose habitat: landscape evaluation. The Journal of Wildlife Management 61: 517–524.

Ruprecht, J. S., D. N. Koons, K. R. Hersey, N. T. Hobbs, and D. R. MacNulty. 2020. The effect of climate on population growth in a cold-adapted ungulate at its equatorial range limit. Ecosphere 11: e03058.

Sala, O. E., F. Stuart Chapin, III, J. J. Armesto, E. Berlow, J. Bloomfield, R. Dirzo, E. Huber-Sanwald, L. F. Huenneke, R. B. Jackson, A. Kinzig, R. Leemans, D. M. Lodge, H. A. Mooney, M. Oesterheld, N. L. Poff, M. T. Sykes, B. H. Walker, M. Walker, and D. H. Wall. 2000. Global Biodiversity Scenarios for the Year 2100. Science 287: 1770–1774.

Schultz, E. A., N. Ellison-Neary, M. R. Boudreau, G. M. Street, L. R. Jones, K. O. Evans, and R. B. Iglay. 2024. On the move: Influence of animal movements on count error during drone surveys. Ecology and Evolution 14: e70287.

Seymour, A. C., J. Dale, M. Hammill, P. N. Halpin, and D. W. Johnston. 2017. Automated detection and enumeration of marine wildlife using unmanned aircraft systems (UAS) and thermal imagery. Scientific Reports 7: 45127.

Solberg, E. J., B.-E. Saether, O. Strand, and A. Loison. 1999. Dynamics of a harvested moose population in a variable environment. Journal of Animal Ecology 68: 186–204.

Spaan, D., C. Burke, O. McAree, F. Aureli, C. E. Rangel-Rivera, A. Hutschenreiter, S. N. Longmore, P. R. McWhirter, and S. A. Wich. 2019. Thermal infrared imaging from drones offers a major advance for spider monkey surveys. Drones 3: 34.

Steinhorst, R. K., and M. D. Samuel. 1989. Sightability adjustment methods for aerial surveys of wildlife populations. Biometrics 45: 415–425.

Street, G. M., A. R. Rodgers, and J. M. Fryxell. 2015. Mid-day temperature variation influences seasonal habitat selection by moose. The Journal of Wildlife Management 79: 505–512.

Su, Y.-S., and M. Yajima. 2024. R2JAGS: using R to run "JAGS." <https://cran.r-project.org/web/packages/R2jags/index.html>. Accessed 30 Sep 2024.

Sullivan, F. B., A. G. Hunsaker, M. W. Palace, and J. M. Jacobs. 2023. Evaluating the effects of UAS flight speed on LiDAR snow depth estimation in a heterogeneous landscape. Remote Sensing 15: 5091.

Tape, K. D., D. D. Gustine, R. W. Ruess, L. G. Adams, and J. A. Clark. 2016. Range expansion of moose in arctic Alaska linked to warming and increased shrub habitat. PLOS ONE 11: e0152636.

Teitelbaum, C. S., A. P. K. Sirén, E. Coffel, J. R. Foster, J. L. Frair, J. W. Hinton, R. M. Horton, D. W. Kramer, C. Lesk, C. Raymond, D. W. Wattles, K. A. Zeller, and T. L. Morelli. 2021. Habitat use as indicator of adaptive capacity to climate change. Diversity and Distributions 27: 655–667.

Tyre, A. J., B. Tenhumberg, S. A. Field, D. Niejalke, K. Parris, and H. P. Possingham. 2003. Improving precision and reducing bias in biological surveys: estimating false-negative error rates. Ecological Applications 13: 1790–1801.

Wang, D., Q. Shao, and H. Yue. 2019. Surveying wild animals from satellites, manned aircraft and unmanned aerial systems (UASs): a review. Remote Sensing 11: 1308.

Wiens, J. A. 1989. Spatial scaling in ecology. Functional Ecology 3: 385–397.

Zabel, F., M. A. Findlay, and P. J. C. White. 2023. Assessment of the accuracy of counting large ungulate species (red deer *Cervus elaphus*) with UAV-mounted thermal infrared cameras during night flights. Wildlife Biology 2023: e01071.

Zmarz, A., M. Rodzewicz, M. Dąbski, I. Karsznia, M. Korczak-Abshire, and K. J. Chwedorzewska. 2018. Application of UAV BVLOS remote sensing data for multi-faceted analysis of Antarctic ecosystem. Remote Sensing of Environment 217: 375–388.

Zuur, A. F., E. N. Ieno, and C. S. Elphick. 2010. A protocol for data exploration to avoid common statistical problems. Methods in Ecology and Evolution 1: 3–14.